NJC

ROYAL SOCIETY OF CHEMISTRY

PAPER

View Article Online
View Journal | View Issue

Cite this: *New J. Chem.*, 2021, **45**, 17320

Synthesis, theoretical calculations and laser flash photolysis studies of selected amphiphilic porphyrin derivatives used as biofilm photodegradative materials†

Yolande Ikala Openda,[a] Bokolombe Pitchou Ngoy,[ab] Jules Tshishimbi Muya [b] and Tebello Nyokong *[a]

Photodynamic antimicrobial activities of gallium and indium porphyrins as well as their quaternized derivatives have been investigated against *S. aureus* and *E. coli* biofilms, as well as on their planktonic (free floating) cells using a light emitting diode lamp at 415 nm. The studied photosensitizers show considerable ability to generate singlet oxygen and the quaternized molecules **2a** and **3a** are potential photodynamic antimicrobial chemotherapy (PACT) agents with $\log_{10}$ colony forming units >9 for *E. coli* and *S. aureus* planktonic cells. The quaternized derivatives are found to have higher ability to significantly suppress the biofilms of both *S. aureus* and *E. coli in vitro*. Therefore, this demonstrates that they are potentially suitable photosensitive agents for PACT use. The TD-B3LYP/LanL2DZ calculations were performed to evaluate the singlet excitation energies of quaternized and non-quaternized porphyrins *in vacuo*. Our study shows excellent agreement between time-dependent density-functional theory (TD-DFT) excited energies and experimental S1 > S0 excitation energies. The small deviation observed between the calculated and experimental spectra arises from the solvent effect. The excitation energies observed in these UV-visible spectra mostly originated from electron promotion between the highest occupied molecular orbital (HOMO) for the less intense band and the HOMO−1 for the most intense band of the ground states to the lower unoccupied molecular orbital (LUMO) of the excited states.

Received 30th May 2021,
Accepted 12th August 2021

DOI: 10.1039/d1nj02651h

rsc.li/njc

Introduction

In nature, the majority of bacteria do not exist as freely suspended cells but they occur as surface-aggregated communities known as biofilms. In fact, bacterial cells can attach to inert and living surfaces, medical devices, industrial systems, outdoor constructions, maritime structures and piping systems.[1,2] The polymicrobial communities living within biofilms are enclosed in an extracellular polysaccharide layer which plays multiple roles including protection against desiccation, immune targeting and antibiotic treatments.[3,4] Biofilm formation is a crucial virulence mechanism in the pathogenesis of many microbial pathogens such as *Staphylococcus aureus*[5] and *Escherichia coli*.[6]

Biofilms are a subject of great concern to the scientific world, as not only are they linked to most severe infections in humans, but they are also very difficult to eradicate due to their characteristic tolerance to immune responses and resistance to commonly used antimicrobials.[7–9] Therefore, to delay biofilm formation or to remove installed biofilms, with minimum impact on the host or environment, different strategies are being intensively explored.

Recently, the photodynamic antimicrobial chemotherapy (PACT) process has risen as an effective antimicrobial approach used to lessen concerns about antibiotic resistance and to replace or/and to back up antibiotic treatments. During PACT, a photosensitizer (PS) absorbs light of appropriate wavelength and quickly goes to the triplet state (T_1) through intersystem crossing (ISC) where it transfers the absorbed energy to the ground-state molecular oxygen. This results in the generation of free radicals (Type-I reaction) or the cytotoxic singlet oxygen ($^1O_2$) *via* Type-II reaction,[10] which causes oxidative damage to the target cell.[11–13] Hence, there is a need to develop novel and efficient photosensitizers (PSs) for use in PACT.

However, reports have proven that singlet oxygen production and cell death are not always correlated, but rather the toxicity of PACT depends on the subcellular localization of the PS.[14] Therefore, to improve the PS affinity or localization in bacteria cells, we introduced lipophilicity by quaternization since

[a] *Institute for Nanotechnology Innovation, Department of Chemistry, Rhodes University, Makhanda 6140, South Africa. E-mail: t.nyokong@ru.ac.zal; Fax: + 27 46 6225109; Tel: +27 46 6038260*
[b] *Département de Chimie, Université de Kinshasa, Kinshasa, Democratic Republic of the Congo*

† Electronic supplementary information (ESI) available. See DOI: 10.1039/d1nj02651h

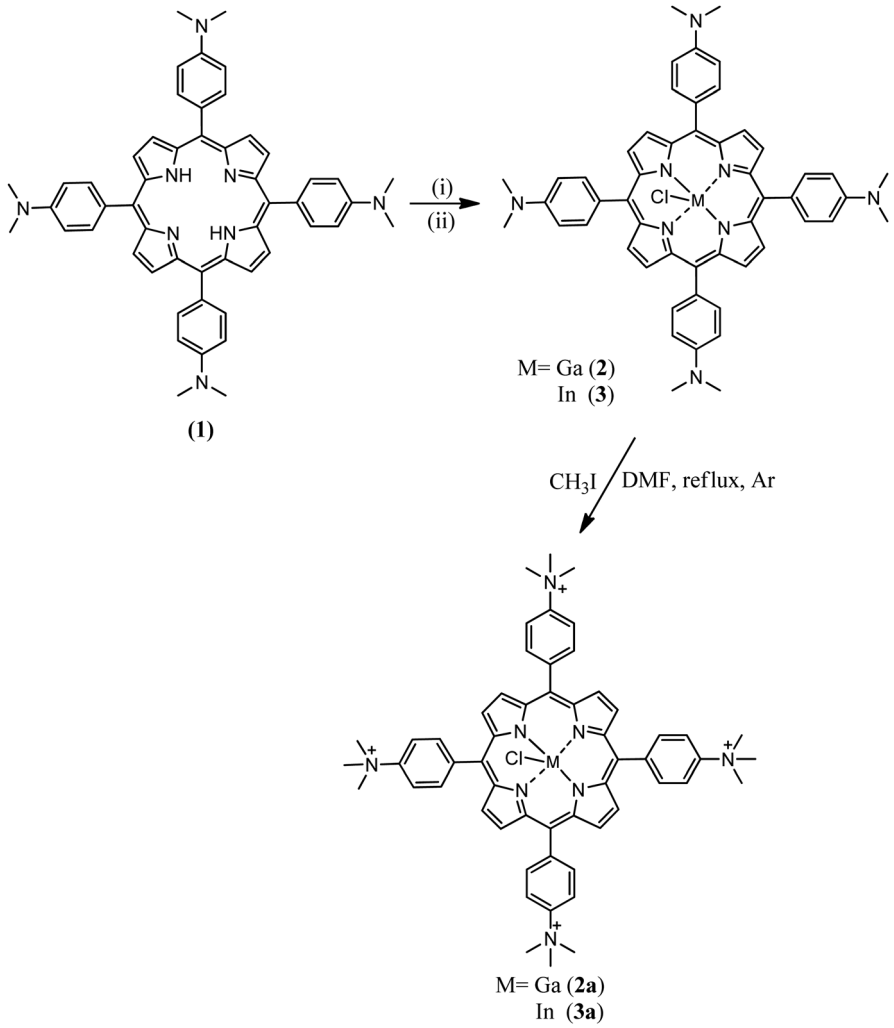

Scheme 1 The synthesis routes of porphyrin derivatives. Reaction conditions: (i): $GaCl_3$, dry DMF, reflux, and Ar; (ii) anhydrous $InCl_3$, NaOAc, glacial acetic acid, reflux, and Ar.

cationic PSs can proficiently target both Gram(−) and Gram(+) bacteria by enhancing the permeability of the outer wall[15–17] and localizing in the mitochondria where the concentration of oxygen is high.[18]

We report on the synthesis of indium(III) and gallium(III) dimethylamino-tetrasubstituted porphyrins along with quaternized counterparts. The choice of these heavy central metals is based on the fact that they improve ISC to the triplet state, thus resulting in a higher singlet oxygen quantum yield.[19] Most studies on PACT using porphyrins have been using planktonic bacteria with only a few reports on biofilms, but using metal-free neutral or quaternized porphyrins.[20–22] In this work, we use porphyrins containing heavy In and Ga central metals for PACT on biofilms. We employ the neutral (**2**, **3**, Scheme 1) and quaternized (**2a**, **3a**, Scheme 1) porphyrin derivatives in this work.

Photodynamic antimicrobial chemotherapy of novel metalated porphyrins on the gram(+) bacteria, *S. aureus*, and gram(−) bacteria, *E. coli*, planktonic cells and biofilms was assessed. The TD-B3LYP/LanL2DZ calculations were also achieved to estimate the singlet excitation energies of quaternized and non-quaternized porphyrin derivatives *in vacuo*.

Experimental

Materials

Tetraphenyl-porphyrin (TPP), anhydrous indium(III) chloride, gallium(III) chloride, sodium acetate (NaOAc), 9,10-dimethylanthracene (DMA), 9,10-antracenediyl-bis(methylene) dimalonoic acid (ADMA), iodomethane, Rose Bengal (RB), tryptic soy broth and crystal violet were purchased from Sigma-Aldrich. Dimethylformamide (DMF), dimethylsulfoxide (DMSO), and tetrahydrofuran (THF), including all other reagents, were used as received from the suppliers unless otherwise stated. *Staphylococcus aureus* and *Escherichia coli* were obtained from Davies Diagnostics, South Africa. Nutrient agar and nutrient broth used in the present study were from Merk (Pty) Ltd, South Africa. Phosphate buffer saline (10 mM PBS, pH 7.4) was prepared using appropriate amounts

of Na_2HPO_4 and NaOH with highly purified H_2O from ELGA, Veolia water PURELAB, Flex system (Marlow, UK).

Equipment

A Shimadzu UV-2250 spectrophotometer was used to record absorption spectra and to perform singlet oxygen experiments. The ^{1}H NMR spectra in deuterated DMSO were obtained using a Bruker® AVANCE 400 MHz NMR spectrometer. The mass spectra were recorded with a Brucker AutoFLEX III Smartbeam TOF/TOF mass spectrometer in the positive mode using alpha-cyano-4-hydroxycinnamic acid as a MALDI matrix. Infrared spectroscopy was carried out using a Bruker Alpha IR (100 FT-IR) spectrophotometer with universal attenuated total reflectance (ATR). Fluorescence measurements were performed with a Varian Eclipse spectro-fluorimeter.

The triplet lifetimes (τ_T) were obtained using a laser flash photolysis system consisting of an LP980 spectrometer with a PMT-LP detector and an ICCD camera (Andor DH320T-25F03). The signal from the PMT detector was recorded with a Tektronix TDS3012C digital storage oscilloscope. The excitation pulses were produced using a tunable laser system consisting of an Nd:YAG laser (355 nm, 135 mJ/4–6 ns) and an optical parametric oscillator (OPO, 30 mJ/3–5 ns) with a wavelength range of 420–2300 nm (NT-342B, Ekspla). The data were determined by the exponential fitting of the kinetic curve using Origin Pro 8 software.

An energy-dispersive X-ray spectrometer (EDX, INCA PENTA FET coupled with a VAGA TESCAM operated at 20 kV) was utilized to qualitatively determine the elemental compositions of the studied complexes.

The conductivity studies were performed using a 86555 AZ Benchtop multiparameter water quality meter – pH/ORP/conductivity/TDS/salinity with a printer.

Regarding PACT experimentation, a Merck Eppendorf centrifuge 5810 was used to harvest bacteria cells. A PRO VSM-3 Labplus Vortex mixer was used to homogenize the bacterial suspensions and a thermostatic oven was used for incubation. The optical density (OD) of bacteria was obtained from LEDETECT 96. The illumination studies were conducted using a 415-nm LED lamp. The colony forming unit (CFU mL^{-1}) counting was perfomed with a Scan® 500. A Synergy 2 multimode microplate reader (BioTek1) with an excitation wavelength of 590 nm was used for biofilm quantification.

Synthesis

Synthesis of metalloporphyrins (Scheme 1)

The preparation of free-base porphyrin **1** has been reported in the literature.[23]

Chloro gallium 5,10,15,20-tetrakis(4-dimethylaminophenyl)-porphyrin (2). Under an argon atmosphere, the free base compound **1** (0.100 g, 0.13 mmol) was stirred in refluxing DMF until complete dissolution. Afterwards, anhydrous gallium chloride (0.081 g, 0.46 mmol) was added to the solution which was left to stir until completion as confirmed by UV/Vis spectrophotometry by checking the collapse of the four Q-bands in the spectrum of complex **1** to the two bands of complex **2**. Once completed, the mixture was cooled to room temperature, and then ethanol/water mixture (50 mL, 1 : 1 v/v) was added in order to precipitate out the corresponding porphyrin **2**. The precipitate was filtered off under a vacuum, washed with millipore water and dried *in vacuo*. The MALDI-TOF MS data and ^{1}H NMR data were in agreement with the suggested structure.

Yield: 106 mg (96%). FT-IR: ν, cm^{-1} 3013–2996 (Alph. and Ar. C–H stretches), 1605 (C═N and C═C stretches), 1488–1428 (C–H bend), 1107 (C–N stretch) and 985 (═C–H bend). ^{1}H NMR (400 MHz, DMSO-d_6): δ_H, ppm 8.23 (d, J = 8.3 Hz, 8H, Ar-H), 7.93 (d, J = 8.4 Hz, 2H, pyrrole-H), 7.68 (d, J = 8.3 Hz, 8H, Ar-H), 7.30 (d, J = 7.8 Hz, 2H, pyrrole-H), 6.78 (d, J = 8.0 Hz, 4H, pyrrole-H) and 3.04 (s, 24H, –CH_3). MALDI TOF-MS, calc. 890.17, found 891.40 $[M + H]^+$ and 856.37 $[M + H - Cl]^+$. UV/visible (DMSO), λ_{max} nm (log ε): 423 (5.6), 561 (3.6), 600 (2.9).

Chloro indium 5, 10, 15, 20-tetrakis(4-dimethylaminophenyl)-porphyrin (3). Porphyrin **1** (0.1 g, 0.13 mmol) was first dissolved in glacial acetic acid (20 mL) under an argon atmosphere and the mixture was stirred at refluxing temperature before adding indium chloride (0.141 g, 0.64 mmol) and sodium acetate (0.381 g, 4.6 mmol). After the completion of the reaction, the mixture was cooled to room temperature and then poured into ice water to obtain a green precipitate, which was filtered off under vacuum, washed with water and dried *in vacuo*.

Yield: 99 mg (83%). FT-IR: ν, cm^{-1} 2847 (Alph. and Ar. C–H stretches), 1605 (C═N and C═C stretches), 1556 (C–H bend), 1164 (C–N stretch) and 963 (═C–H bend). ^{1}H NMR (400 MHz, DMSO-d_6): δ_H, ppm 8.27 (d, J = 8.2 Hz, 8H, Ar-H), 7.91 (*d*, J = 8.0 Hz, 2H, pyrrole-H), 7.73 (d, J = 8.1 Hz, 8H, Ar-H), 7.27 (d, J = 8.1 Hz, 2H, pyrrole-H), 6.78 (d, J = 8.1 Hz, 4H, pyrrole-H) and 3.06 (s, 24H, –CH_3). MALDI TOF-MS, calc. 935.26, found 936.10 $[M + H]^+$. UV/visible (DMSO), λ_{max} nm (log ε): 431 (5.7), 567 (3.7), 605 (3.4).

Synthesis of the quaternized metalloporphyrins 2a and 3a. Complexes **2** and **3** were quaternized following a procedure reported in the literature with slight modifications,[24] where an excess of iodomethane (4 mL) was mixed with **2** (0.050 g, 0.056 mmol) or **3** (0.050 g, 0.053 mmol), and the mixtures were dissolved in dry DMF (3 mL). Each of the reaction mixtures was refluxed for 72 h under an argon atmosphere and the desired products (**2a**, **3a**) were obtained after precipitation with acetone and centrifugation at 3500 rpm for 5 min.

Complex 2a. Yield: 52 mg (97%). FT-IR: ν, cm^{-1} 3013–2995 (Alph. and Ar. C–H stretches), 1606 (C═N and C═C stretches), 1482 (C–H bend), 1116 (C–N stretch) and 944 (═C–H bend). ^{1}H NMR (400 MHz, $CDCl_3$): δ_H, ppm 7.75 (d, J = 7.5 Hz, 8H, Ar-H), 7.72 (d, J = 8.0 Hz, 8H, Ar-H), 7.65 (d, J = 7.6 Hz, 2H, pyrrole–H), 7.57 (d, J = 8.4 Hz, 4H, pyrrole–H), 7.40 (d, J = 7.9 Hz, 2H, pyrrole–H) and 3.10 (s, 36H, –CH_3). UV/visible (DMSO), λ_{max} nm (log ε): 428 (5.9), 564 (3.9), 600 (3.4).

Complex 3a. Yield: 49 mg (93%). FT-IR: ν, cm^{-1} 28475 (Alph. and Ar. C–H stretches), 1606 (C═N and C═C stretches), 1556 (C–H bend), 1163 (C–N stretch) and 961 (═C–H bend).

^{1}H NMR (400 MHz, $CDCl_3$): δ_H, ppm 7.77 (d, J = 8.1 Hz, 8H, Ar-H), 7.73 (d, J = 7.5 Hz, 8H, Ar-H), 7.67 (d, J = 7.9 Hz, 2H, pyrrole-H), 7.57 (d, J = 8.4 Hz, 4H, pyrrole-H), 7.40 (d, J = 7.7 Hz, 2H, pyrrole-H) and 3.09 (s, 36H, $-CH_3$). UV/visible (DMSO), λ_{max} nm (log ε): 439 (5.9), 568 (3.7), 609 (3.6).

Photophysicochemical properties

Fluorescence quantum yield (Φ_F) and singlet oxygen quantum yield (Φ_Δ) were determined using comparative methods reported in the literature[25] with equations explained in the ESI.† TPP (Φ_F = 0.14[26] and Φ_Δ = 0.52[27]) was used as a standard in DMSO and DMA was used as a singlet oxygen quencher in DMSO. Rose Bengal (RB) ($\Phi_{\Delta RB}$ = 0.75[28]) was used as a standard and ADMA was used as a singlet oxygen quencher in water (containing 1% DMSO).

Computational method

Geometry optimizations were carried out at the B3LYP/LanL2DZ level with symmetry and no constraints. The optical absorption spectra were computed using TD-B3LYP at the same theoretical level *in vacuo*. This method has been previously used[29] on transition metal compounds and nanoclusters and it has shown to provide optical properties close to experimental ones. The theoretical background of time-dependent density functional theory is described elsewhere.[30] The effect of the solvent was estimated by comparing the experimental results obtained in solvents and the theoretical spectra carried out *in vacuo*. All calculations were performed using the Gaussian 09 program.[31]

Photodynamic antimicrobial chemotherapy studies

Antibacterial assays on planktonic cells. The antibacterial effect of porphyrins was evaluated on *S. aureus* and *E. coli*, following the protocol reported by Openda *et al.*[32] Briefly, bacterial suspensions were aseptically prepared by mixing an aliquot of each bacteria with 5 mL of freshly prepared nutrient broth, followed by incubation at 37 °C for cultivation until the optical density (OD) values at 620 nm were around 0.6–0.8. Afterwards, the resulting cultures were centrifuged (4000 RPM for 15 min) and washed with phosphate buffer solution (PBS) to obtain bacterial pallets. The obtained solids were resuspended in 100 mL PBS to make stock suspensions of 10^{-2} dilution factor. From the stock solution, serial dilutions of 10^{-3}, 10^{-4}, 10^{-5}, 10^{-6} and 10^{-7} were then prepared in order to perform bacteria optimizations. For this, 100 μL of each inoculum were aseptically seeded on agar plates and incubated at 37 °C. After 24h, CFU counting was carried out. 10^{-6} corresponding to the count of 3.02×10^{10} CFU mL^{-1} and 10^{-5} corresponding to the count of 2.01×10^9 CFU mL^{-1} were found as the best to be used for *S. aureus* and *E. coli*, respectively.

Photoinactivation experiments were carried out following a procedure recently described in our laboratory.[33,34] First, porphyrins in DMSO/PBS (1 : 99 v/v) solutions were prepared at 1.25, 2.5, 5, 10, 20 and 40 μg mL^{-1} in order to find the optimal concentrations. Optimal concentrations of 10 μg mL^{-1} and 1.25 μg mL^{-1} were chosen for the non-quaternized and quaternized samples, respectively. Then, a light emitting diode (LED) M415L4 at 415 nm was used as a light source at a constant irradiance of 15.6 μW mm^{-2} for 2 h with 30 min intervals. The experiments were also done in the dark.

Biofilm photodynamic assays

The individual single-species biofilms of *S. aureus* and *E. coli* were made following the experimental procedure[32,34] where tryptic soy broth was used to prepare bacterial inocula of 10^9 CFU mL^{-1}. 200 μL was taken from the suspension and placed in 96-well plates followed by incubation at 37 °C for 5 days. Meanwhile, unbound cells were washed with PBS and the wells were refilled with fresh 200 μL of tryptic soy after 18 h to stimulate biofilm formation. At the end of the process, the biofilm-coated wells were carefully washed twice with PBS and left to air dry for 30 min.

For irradiation, 100 μL from each porphyrin concentration (25, 50 and 100 μg mL^{-1}) was added into biofilm-coated wells and the resulting suspensions were allowed to incubate for 30 min in the dark at 37 °C, before irradiating with a 415-nm LED for 30 min. After irradiation, 200 μL of 1% aqueous crystal violet (CV) solution was added to the wells to stain the cells. After 30 min, the excess CV was washed off thrice with PBS and the wells were refilled with PBS in order to quantify the biofilm survival cells by reading their absorbance.

On the other hand, the suspensions of biofilms with drugs were diluted in PBS and then 100 μL of each solution was aseptically inoculated on agar plates followed by incubation for 18 h at 37 °C. The same was applied for the samples kept in the dark and all the tests were performed in triplicate whereas DMSO/PBS (1 : 99 v/v) solutions served as a positive control.

Statistical analysis

All the experiments were conducted in triplicate using a 3-way factorial ANOVA. The data are represented, in this work, as mean ± standard deviation (SD) of $\log_{10}$ CFU values for the planktonic cells or mean ± SD of cell survival for the biofilms. A p-value of 0.05 was considered statistically significant.

Results and discussion

Synthesis and characterization

In the current work, the synthesis of the new complexes was achieved through the insertion of heavy central metals such Ga(III) and In(III) in the core of the free base porphyrin **1** (Scheme 1). The quaternized derivatives **2a** and **3a** were obtained through methylation reactions of porphyrin complexes **2** and **3** using an excess of iodomethane (CH_3I) in dry DMF at reflux temperature. The characterization of these compounds was carried out using ^{1}H NMR, IR, UV-Vis and MS (see the ESI,† Fig. S1–S4, as examples for MS and NMR and **S5** for energy-dispersive X-ray spectra, EDX) and all the acquired data were in agreement with the predictions.

Complexes **2** and **3** were obtained as purple powders. Complex **2** exhibited a protonated molecular ion peak at

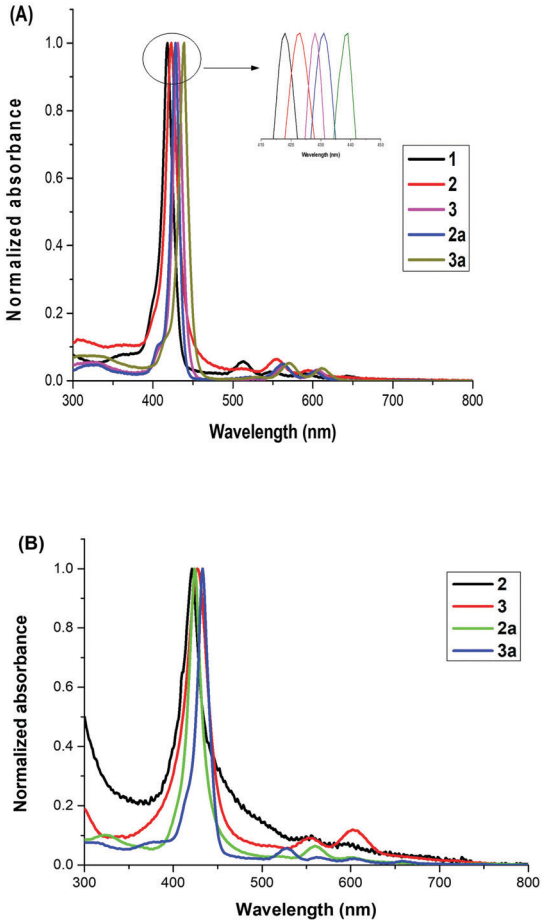

Fig. 1 UV-vis spectra of porphyrins: (A) in DMSO and (B) in DMSO/PBS (1 : 99 v/v).

m/z = 891.40 $[M + H]^+$ and another peak at 956.37 $[M - Cl]^+$, while complex **3** showed m/z = 936.10 $[M + H]^+$ in the MS spectrum (Fig. S1 and S2 in ESI†). The mass spectra of the quaternized porphyrins were not acquired due to the lack of ionisation of these compounds. The ^{1}H NMR spectra for all **2**, **2a**, **3** and **3a** exhibited aromatic proton peaks ranging from 8.23 to 6.78 ppm which integrated for 24 protons. The geminal methyl protons resonated in the aliphatic region between 3.04 and 3.10 (Fig. S3 and S4, ESI,† using complexes **2** and **2a** as examples).

EDX analysis was also used to determine the elemental composition of the complexes. As illustrated in Fig. S5 in the ESI,† C, N, Ga and Cl were present in the spectra of gallium derivatives whereas C, N, In and Cl were obtained for the indium counterparts. The sulphur peak that comes from DMSO which was used for dissolving the porphyrins for coating the grid and drying for EDX spectra.

In addition, the specific conductance data listed in Table S1 in the ESI† prove the non-electrolyte nature of the quaternized complexes as they were in the normal range of typical drinking water (1–1000 μS cm^{-1})[35] even though these values were about 2 times higher than the conductivity of the water used in this case at the same temperature. It has also been reported that

Table 1 Photophysicochemical parameters of the porphyrin derivatives in DMSO

Sample	λ_{abs} [a]	$\lambda_{em.}$	Φ_F	τ_T (μs)	Φ_Δ [a]
1	418	600–774	0.107	246	0.37
2	423 (420)	610–662	0.075	193	0.54 (0.27)
2a	428 (424)	576–680	0.029	176	0.54 (0.29)
3	431 (427)	575–682	0.072	101	0.58 (0.30)
3a	439 (433)	560–580	0.025	58	0.63 (0.33)

[a] Values in brackets are in water (containing DMSO, 1 : 99 v/v) used for cell studies. abs= absorption, em = emission.

molecular complexes, in this case porphyrins, have very poor electrical conductivity.[36]

Fig. 1A illustrates the typical UV-Vis spectra of the synthesized porphyrin derivatives. The B-band of **1** appeared at 418 nm (Fig. 1A and Table 1) with four Q-bands in DMSO. As known from the literature, the spectral red-shifts and the collapse of the four Q-bands for the free base to two confirm successful metalation.[37] In this case, the metalation of **1** was confirmed by the slight red-shifts in the spectra of **2** and **3** to 423 and 431 nm, respectively, from 418 nm for porphyrin **1** (Table 1). The largest shifts were observed for complex **3** due to the non-planar effect of the In(III) ion and its bigger atomic radius compared to that of the Ga(III) ion.[38] There were slight red-shifts in the Soret bands upon the quaternization of **2** and **3** to **2a** and **3a**, respectively (Fig. 1A and Table 1). The spectra obtained in DMSO/PBS (1 : 99 v/v) (used for bacterial studies) showed aggregation as judged by the broadening with

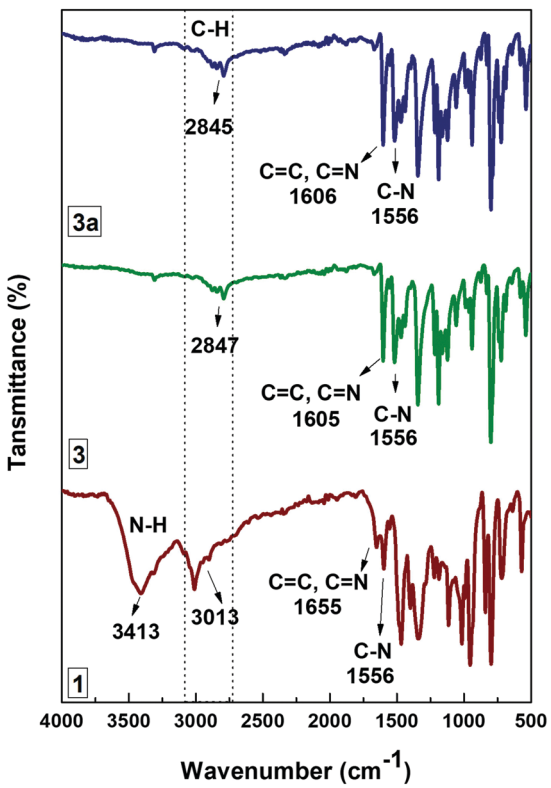

Fig. 2 FT-IR spectra of the selected derivatives.

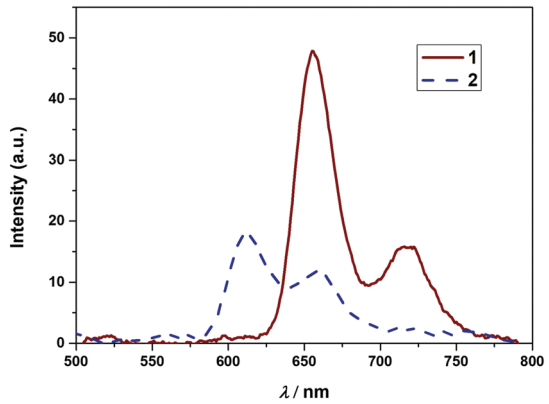

Fig. 3 Typical emission spectra of porphyrins (**1** and **2** used as examples).

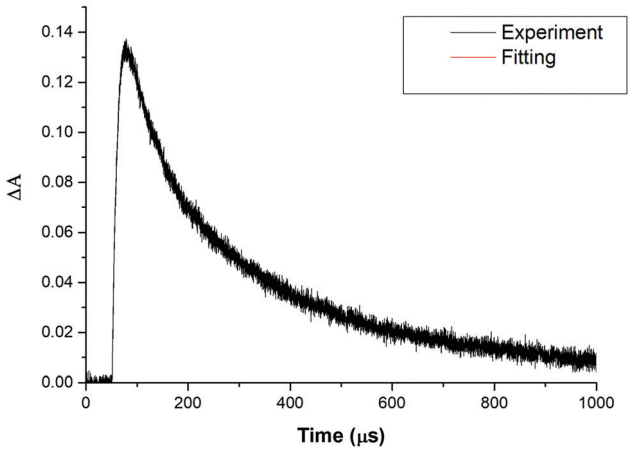

Fig. 5 Transient decay curve (λ_{exc} = 425 nm) of **3** in degassed DMSO (as an example).

blue-shifts, Fig. 1B and Table 1. The FT-IR data are shown in Fig. 2 to trace the modifications of the functional groups present in the molecules. The spectra of porphyrins **2** and **3** did not show N–H peak stretch as observed in the spectra of porphyrin **1** around 3413 cm^{-1}. This confirms that the metalation was successful. As expected, C═C and C═N stretches emerged at about 1605 cm^{-1} and the C–N peak around 1556 cm^{-1} for **2**, **3**, **2a** and **3a**.

Photophysicochemical properties

Emission spectra and fluorescence quantum yield (Φ_F). From Fig. 3 (Table 1) and Fig. S6 in the ESI,† it can be seen that two characteristic bands known for porphyrins are observed in the emission spectra.[37,39] Table 1 shows lower Φ_F values following metalation due to the heavy atom effect of In and Ga.[40]

Singlet oxygen quantum yield (Φ_Δ). Singlet oxygen quantum yield is a quantitative measurement used to compare the ability of different photosensitizers to photogenerate singlet oxygen known as one of the cytotoxic reactive oxygen species. Singlet oxygen photogeneration was indirectly confirmed by monitoring the photobleaching of DMA and ADMA as singlet oxygen scavengers in DMSO and aqueous media, respectively, with irradiation at a cross-over wavelength (420 nm) using the respective standards (Fig. 4 and Fig. S7 in the ESI†). The stability of the porphyrin derivatives was confirmed from Fig. 4 and Fig. S7 (ESI†) where there was no change in the absorption of B-bands after irradiation. The Φ_Δ data are supplied in Table 1 and were in the range of 0.27–0.63 for all the porphyrin derivatives used in this study. The higher Φ_Δ values were obtained for the metalated complexes due to the heavy atom effect[41] and the quaternized **3a** also showed higher Φ_Δ values compared to the corresponding non-quaternized **3** due to the absence of the photoinduced electron transfer (PET) process caused by the unavailability of the lone pair electrons on nitrogen atoms which are bonded to the methyl groups.[10] However, the values are the same for **2** and **2a** in DMSO. The singlet oxygen quantum yield values are lower in water since oxygen has a higher solubility in many organic solvents compared to water.[42] The ability of these complexes to generate singlet oxygen and their hydrophilic properties make them useful for PACT studies.

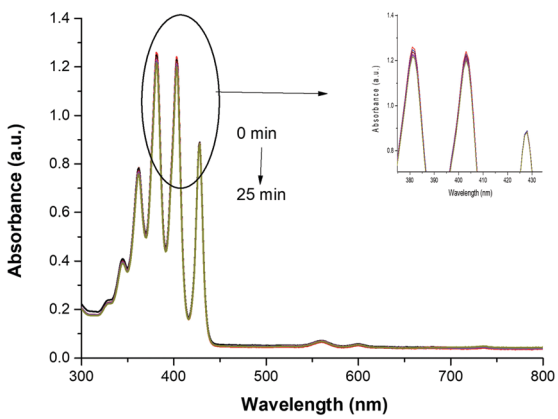

Fig. 4 Typical photodegradation spectra of DMA in the presence of **3** in DMSO.

Laser flash photolysis. Laser flash photolysis studies of compounds led to the formation of transient decay lifetime curves in degassed DMSO solutions (Fig. 5 and Fig. S8 (ESI†) as examples). The triplet lifetime (τ_T) is an important photophysical parameter used to determine the time that the excited molecules spend in the triplet state before they return to the ground state. The quaternized complexes resulted in lower τ_T values (Table 1), compared to their non-quaternized counterparts. The triplet lifetime values are in the range of 58–246 μs (Table 1). The triplet lifetimes of porphyrin derivatives have been reported to be in the microsecond scale in other solvents.[43,44]

TD-DFT results

Quaternized and non-quaternized porphyrin derivatives **1**, **2**, **3**, **1a**, **2a** and **3a** were built in D_{2h} and D_{4h}, respectively. Fig. 6 shows the geometries of porphyrins **1** and **3** as examples. The geometry optimizations reveal that **1** and **1a** keep their high D_{2h} symmetry whereas **2**, **2a** and **3**, **3a** were found unstable

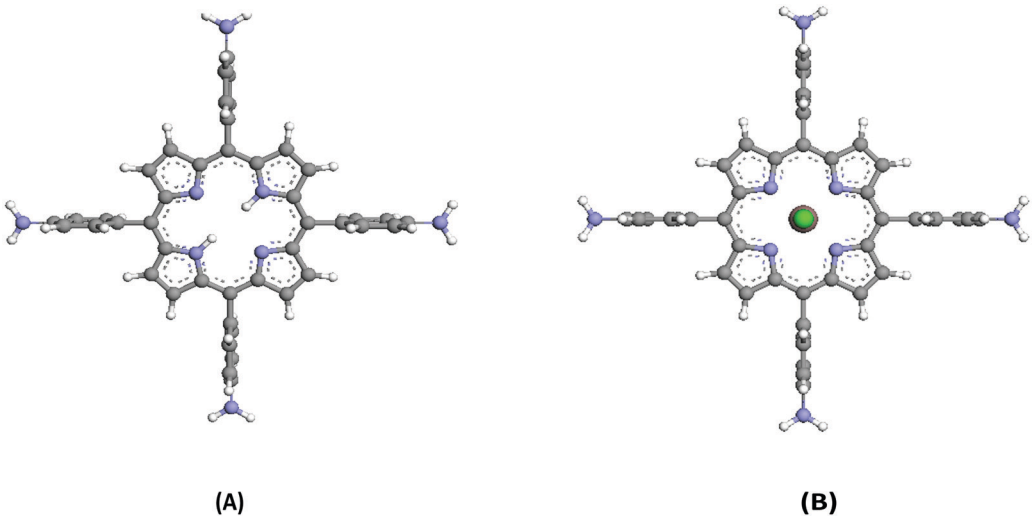

Fig. 6 Initial geometry of porphyrin (A) **1** built in D_{2h} and (B) **3** built in D_{4h}.

in D_{4h} symmetry and undergo symmetry breaking towards the epikernel C_{4v} owing to the pseudo-Jahn–Teller effect. The energy differences between the quaternized and non-quaternized compounds were computed to have a glimpse at the basicity of these compounds (Table 2).

The energy difference illustrated in Table 2 suggests **1** and **3** derivatives to be the most and least basic molecules, respectively. The optical spectra of the studied compounds have the same features so in the present paper we only reported the optical spectrum of complex **3**. Fig. 7 shows the computed UV-visible spectrum of compound **3**. This spectrum is similar to the normalized experimental spectrum. Two regions can be noticed in the spectrum.

A region of strong absorptivity, the B-band region between 300 and 450 nm, and a region of low absorptivity, the Q-band region between 475 and 650 nm, were observed. The deviation between the experiment and TD-DFT excitation energies is quite small ranging between 50 and 28 nm, respectively, for both regions (Table 3) and illustrates the influence of the DMSO solvent. It is to be noted that the calculations were performed *in vacuo* while the experimental data reported here were obtained in solution. The TD-DFT analysis of the most important configuration with the largest coefficient in the excited state reveals that the bands observed originate from electron transfer between the highest occupied molecular orbital (HOMO) and HOMO−1 of the ground state configuration and the lowest unoccupied molecular orbital (LUMO) of the excited configuration. Table 3 lists the excitation energies, oscillator strengths and molecular orbital contributions of the UV-vis spectrum of compound **3** in the gas phase.

Table 2 Total electronic energies in Hartrees of quaternized and non-quaternized porphyrin derivatives and their energy differences in kcal mol^{-1} computed at B3LYP/LanL2DZ

Sample	Quaternized	Non-quaternized	Energy diff in kcal
1	−2136.32953	−2135.096169	−773.94
2	−4518.46774	−4517.250763	−763.67
3	−2151.8155	−2150.611677	−755.41

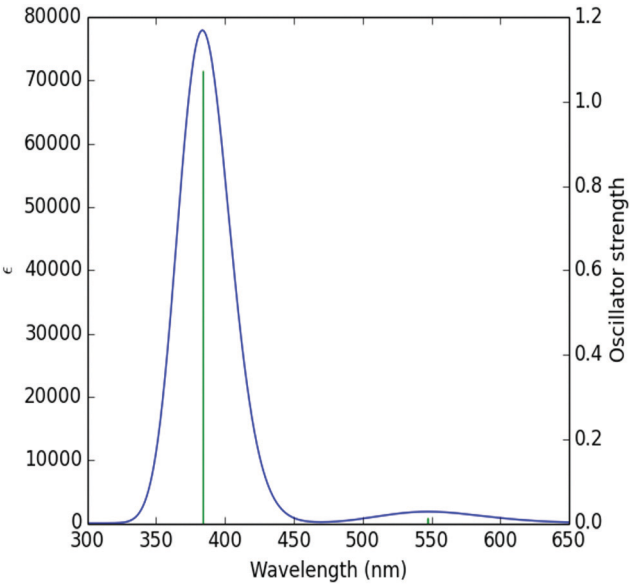

Fig. 7 UV-vis spectra of complex **3** computed at TDB3LYP/LanL2DZ.

Table 3 Excitation energies, oscillator strengths and most important electronic configurations in % that span the excited state wave function of compound **3** computed at TD-B3LYP/LanL2DZ *in vacuo*

	Excited energies in nm	Oscillator strengths	Contribution of MOs in %	Exp.
B-band	383.62	1.075	H−1→ L (54.88%) H → L (35.96%) H−15 → L (8.2%)	431
Q-band	547.49	0.013	H → L(60.73%) H−1 → L(38.55%)	575 682

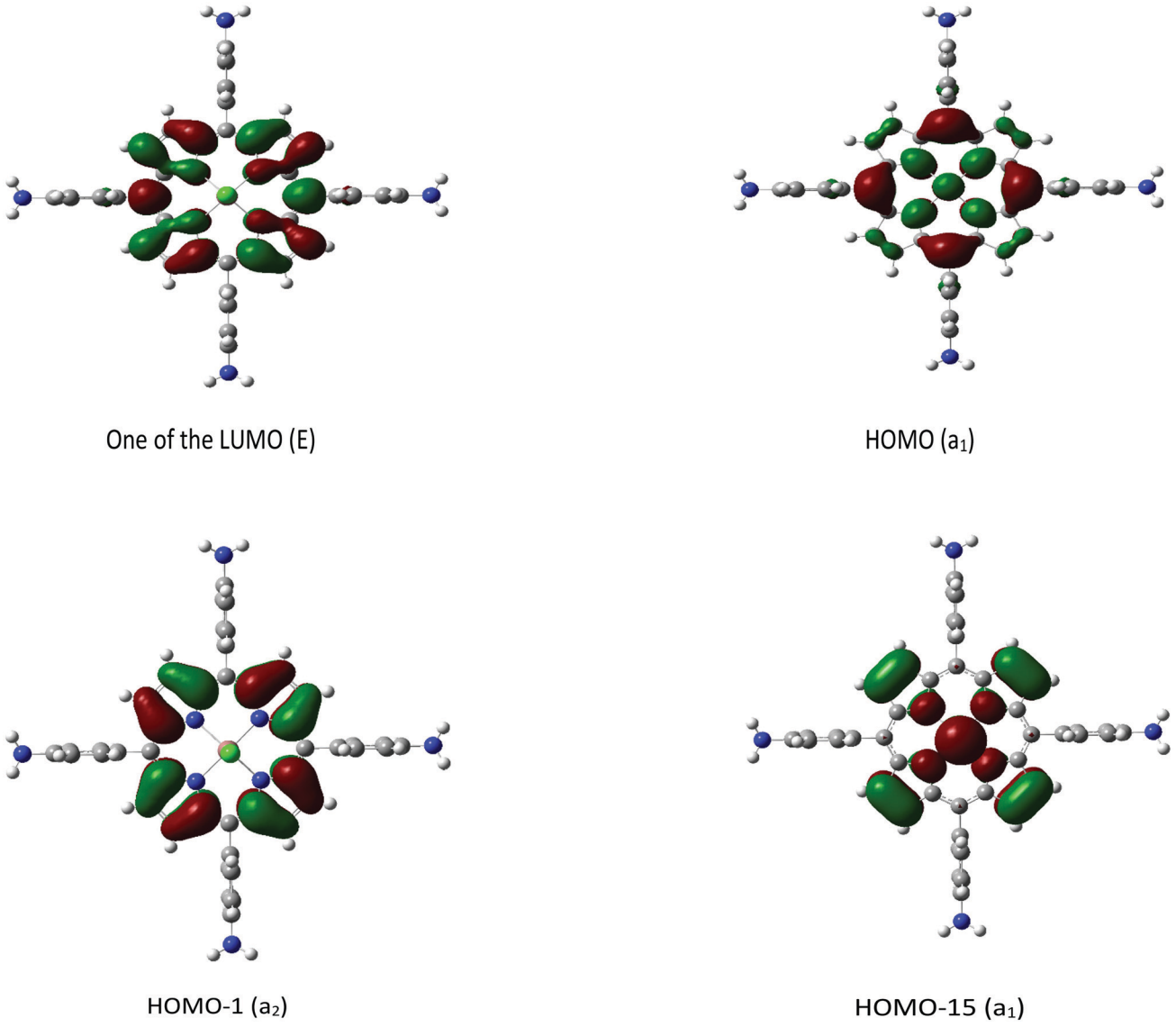

Fig. 8 Frontier molecular orbitals of **1–3**.

While the contribution of the HOMO−1 is the most important in the most intense band (B-band), in the low energy band (Q-band, the less intense band), the largest contribution comes from the promotion of the HOMO to the LUMO orbital. The frontier molecular orbitals of complex **3** and the HOMO−15 orbital are shown in Fig. 8.

The HOMO and HOMO−15 are totally symmetric whereas the LUMO has *E* symmetry and all have predominantly π character. The HOMO and LUMO are, respectively, bonding and anti-bonding orbitals. Thus, all the transitions observed are from π to π*.

Photodynamic antimicrobial studies

The photogeneration of reactive oxygen species, especially singlet oxygen, is one of the main requirements for a photosensitizer to be suitable and efficient for PACT. It was reported in the literature that the hydrophilicity and positive charge in photosensitisers facilitate binding towards negatively charged bacterial cell walls such as *E. coli*, and prevent aggregation in an aqueous medium thus maximizing the cell uptake.[45–47] The bacteria of choice in the current study are *S. aureus* and *E. coli*.

Evaluation of photoinactivation on planktonic cells

The control solutions were prepared with DMSO/PBS (1 : 99 v/v) without photosensitizers. Fig. 9 and 10 illustrate that the irradiated and non-irradiated control solutions of DMSO/PBS (1 : 99 v/v) containing bacteria without photosensitizers showed no activity against microorganisms. The same trend was observed when a solution of DMSO/PBS (1 : 99 v/v) containing bacteria with photosensitizers was kept in the dark as there was no significant change in $\log_{10}$ (CFU, colony forming units) values except for **2a** and **3a** complexes which exhibited slight dark toxicity effects on *S. aureus* with $\log_{10}$ CFU mL^{-1} of 1.26 and 1.32, respectively, whereas on *E. coli* their $\log_{10}$ CFU mL^{-1} were of 1.05 and 1.13 (Fig. 9B and 10B).

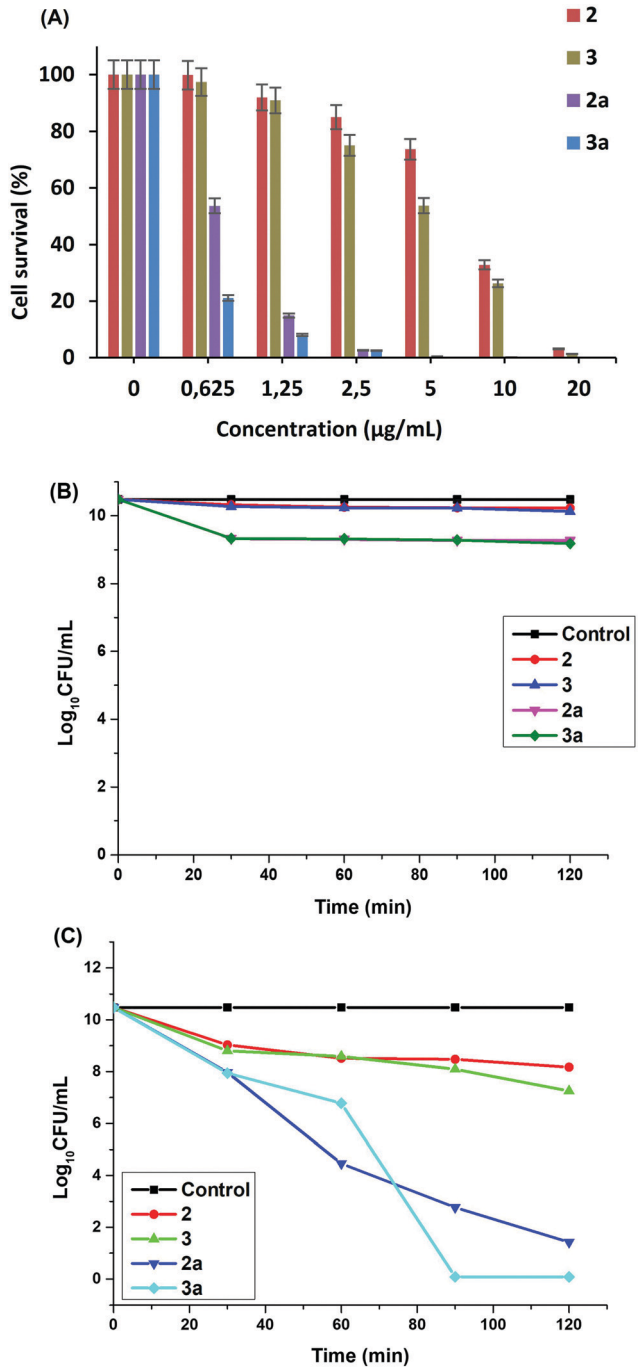

Fig. 9 (A) Cell survival at different concentrations upon 30 min of irradiation and $\log_{10}$ CFU graphs for (B) dark toxicity and (C) PACT studies for *S. aureus* planktonic cells with irradiation at 415 nm. Concentration of the drugs: 10 μg mL^{-1} for non-quaternized and 1.25 μg mL^{-1} for quaternized derivatives. Data are represent as mean ± SD.

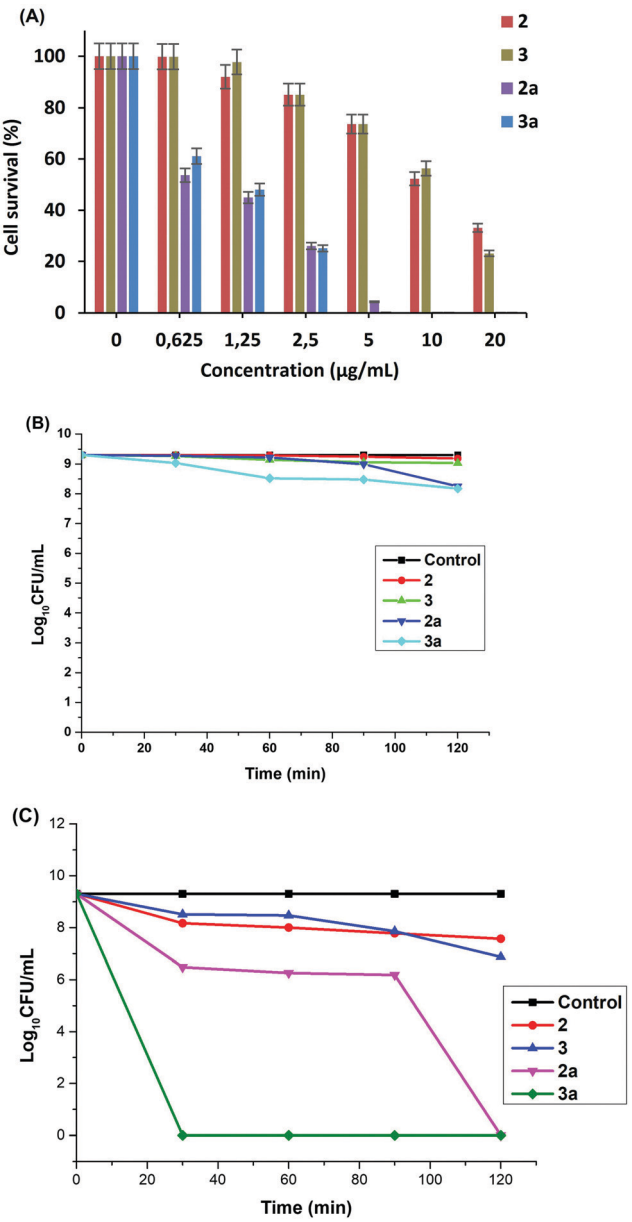

Fig. 10 (A) Cell survival at different concentrations upon 30 min of irradiation and $\log_{10}$ CFU graphs for (B) dark toxicity and (C) PACT studies for *E. coli* planktonic cells with irradiation at 415 nm. Concentration of the drugs: 10 μg mL^{-1} for non-quaternized and 1.25 μg mL^{-1} for quaternized derivatives. Data are represented as mean ± SD.

The antibacterial activities were analysed for all the synthesized porphyrin derivatives and were tested up to 120 min of irradiation duration at 30 min interval with concentrations of 10 μg mL^{-1} and 1.25 μg mL^{-1} for the non-quaternized and quaternized derivatives, respectively.

From the results shown in Fig. 9C and 10C, it is clearly seen that the quaternized complexes had the highest antimicrobial activity on both types of bacteria. The corresponding $\log_{10}$ CFU mL^{-1} values for **2a** and **3a** were around 9.06 and 10.48 against *S. aureus* after 120 and 90 min of irradiation time, respectively (Table 4). For *E. coli*, **2a** and **3a** gave 9.30 $\log_{10}$ CFU mL^{-1} counts after 120 and 30 min of irradiation, respectively. However, the non-quaternized complex **3** exhibited good antibacterial activities with log reduction values of 3.23 against *S. aureus* and 2.43 against *E. coli* after 120 min of irradiation time, compared to complex **2** that had 2.31 $\log_{10}$ CFU mL^{-1} on *S. aureus* and 1.73 $\log_{10}$ CFU mL^{-1} counts on *E. coli* after 120 min of irradiation (Table 4). The high activity of **2a** and **3a** with 0% viable colony comparated to **2** and **3** could be

Table 4 Log reduction and % survival data of 10 μg mL^{-1} for non-quaternized and 1.25 μg mL^{-1} for quaternized samples in DMSO/PBS (1 : 99 v/v) after irradiation

	S. aureus			*E. coli*		
Sample	Log reduction	% Survival	Time of irradiation (min)	Log reduction	% Survival	Time of irradiation (min)
2	2.31	0.40	120	1.73	1.91	120
3	3.23	0.29	120	2.43	0.38	120
2a	9.06	0.008	120	9.30	0	120
3a	10.48	0	90	9.30	0	30

Table 5 The % survival data of samples in DMSO/PBS (1 : 99 v/v) after 30 min of irradiation on *S. aureus* and *E. coli* biofilms

	Cell survival (%)					
	S. aureus			*E. coli*		
Sample	25 μg mL^{-1}	50 μg mL^{-1}	100 μg mL^{-1}	25 μg mL^{-1}	50 μg mL^{-1}	100 μg mL^{-1}
2	91	73	44	91	73	44
3	65	52	8.4	61	39	8.4
2a	26	8.4	2.2	26	8.2	2.0
3a	2.5	2.3	1.6	15	7.6	2.1

due to their hydrophilic nature enabling their attachment to the bacteria cell wall.[15]

It was previously reported that PACT efficiency could be attributed to the ability of the drug to produce singlet oxygen and to the number of cationic charges.[48,49] This is because the cationic charge on a photosensitizer allows stronger affinity to the cell wall and this results in the generation of singlet oxygen in a close proximity of the bacteria cell. This explains the trend observed in this work, where significant toxicity was obtained for cationic complexes on both bacteria, more especially on the gram(−) *E. coli* which is well known as very difficult to treat using neutral or negatively charged photosensitizers.[50]

***In vitro* biofilm eradication.** The extracellular polymeric matrix that envelops cells living within biofilms plays the role of lowering the sensitivity of these cells toward antimicrobial treatment.[51] This implies that higher dosage of drugs should be used in comparison to the treatment of the planktonic cells. Therefore, concentrations of 25, 50 and 100 μg mL^{-1} for each compound were used in this study to evaluate the antibiofilm activity for 30 min of irradiation time using an LED of 415 nm.

Researchers have proved that *S. aureus* and *E. coli* are strong biofilm producers, thus these bacteria were used to form the biofilms of interest following previous reports.[30,52] Table 5 lists the obtained data in percentage survival of all the porphyrins after light treatment.

In Fig. 11A and 12A, it is seen that all the compounds did not kill bacteria in the dark even with high concentrations of drugs. In contrast, Fig. 11B and 12B show that the quaternized derivatives significantly photoinhibited *S. aureus* and *E. coli* biofilms at 100 μg mL^{-1} with 2.2% and 2.0% survival for **2a**, respectively, and 1.6% and 2.1%, for **3a**, while at 50 μg mL^{-1} they showed moderate % cell survival, Table 5. *S. aureus* possessing one single membrane layer is more prone to the antibacterial effect than *E. coli*. However, Table 5 shows that in some cases *E. coli* performed slightly better than *S. aureus*, for example, for **2a** at 100 μg mL^{-1} and 50 μg mL^{-1}.

To the best of our knowledge, this work reports for the first time the eradication of gram(+) and gram(−) biofilms using gallium and indium cationic dimethylamino porphyrins by means of photodynamic antimicrobial chemotherapy. We could expect that these complexes inhibit bacterial cell metabolism and growth, damage

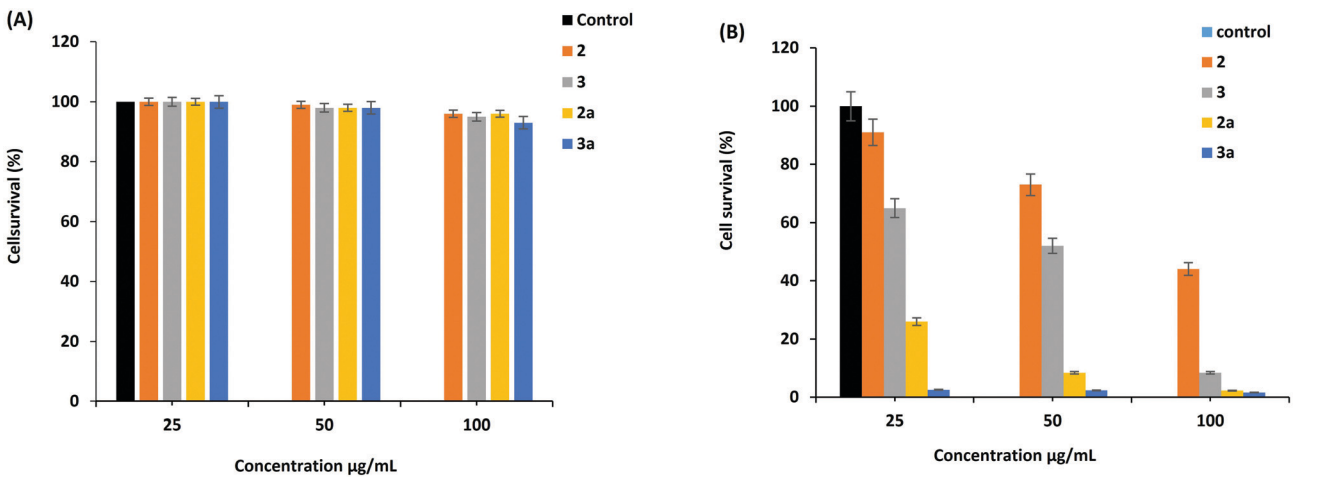

Fig. 11 Cell survival graphs for (A) dark toxicity and (B) PACT studies for *S. aureus* biofilms with irradiation at 415 nm for 30 min. Concentration of the drugs: 25, 50 and 100 μg mL^{-1}. Data are represented as mean ± SD.

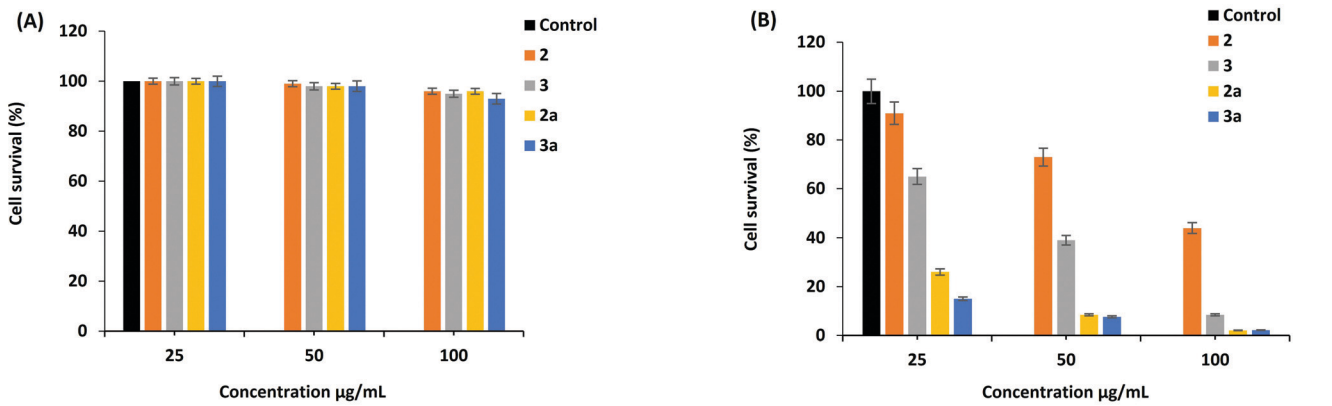

Fig. 12 Cell survival graphs for (A) dark toxicity and (B) PACT studies for *E. coli* biofilms with irradiation at 415 nm for 30 min. Concentration of the drugs: 25, 50 and 100 µg mL^{-1}. Data are represented as mean ± SD.

the cytoplasmic membrane and increase the cell permeability thanks to their cationic charges.[53,54] With this, we can suggest the newly prepared complexes as potential photoantibacterial agents against *S. aureus* and *E. coli*.

Conclusions

To efficiently kill bacteria, positively charged compounds are suggested as they are not only soluble in aqueous media, but they are also able to strongly bind to the cell wall. As a result of this, the cell membrane is highly destroyed since singlet oxygen generated by the photosensitizer acts in close proximity to the cell thus improving the drug-cell uptake. For the same reason in this work, we reported for the first time on novel metalloporphyrins and their amphiphilic derivatives capable of generating high singlet oxygen and eradicating *S. aureus* and *E. coli* bacterial planktonic cells and the most difficult bacterial biofilms following photoinactivation at 415 nm. The readily synthesized complexes were characterized and their photophysicochemical parameters were determined. It was noticed that the PACT results were all in agreement with the reported photophysicochemical results. The *in vitro* results indicate that even with low concentrations and short irradiation time, the studied photosensitisers have great effects on bacterial ablation.

Author contributions

YO made substantial contributions to the synthesis of the metalated porphyrins **2**, **3**, **2a** and **3a**, design, acquisition, analysis, and interpretation of data and took part in the drafting of the manuscript. BN made significant contributions to the design and synthesis of the free base porphyrin **1** and also participated in the writing of the manuscript. JM made great contributions to the manuscript with theoretical calculations. TN made considerable contributions to provide the resources, conceptualized and supervised the work and was the corresponding author in preparing the manuscript. All authors gave their final consent of the submitted manuscript.

Conflicts of interest

There are no conflicts to declare.

Acknowledgements

This work was supported by the Department of Science and Technology (DST) Innovation and National Research Foundation (NRF), South Africa through DST/NRF South African Research Chairs Initiative for Professor of Medicinal Chemistry and Nanotechnology (UID 62620), Rhodes University, the Organization for Women in Science for the Developing World (OWSD) and the Swedish International Development Cooperation Agency (Sida).

References

1 S. Beirao, S. Fernandes, J. Coelho, M. A. F. Faustino, J. P. C. Tome, M. G. P. M. S. Neves, A. C. Tome, A. Almeida and A. Cunha, *Photochem. Photobiol.*, 2014, **90**, 1387–1396.
2 R. M. Donlan, *Emerging Infect. Dis.*, 2002, **8**, 881–890.
3 A. Clinton and T. Carter, *Lab. Med.*, 2015, **46**, 277–284.
4 H. C. Flemming, T. R. Neu and D. J. Wozniak, *J. Bacteriology*, 2007, 7945–7947.
5 R. J. Gordon and F. D. Lowy, *Clin. Infect. Dis.*, 2008, **46**, S350–S359.
6 C. Beloin, A. Roux and J. M. Ghigo, *Curr. Top. Microbiol. Immunol.*, 2008, **322**, 249–289.
7 A. D. Verderosa, M. Totsika and K. E. Fairfull-Smith, *Front. Chem.*, 2019, **7**, 824.
8 R. D. Wolcott and G. D. Ehrlich, *J. Am Med. Assoc.*, 2008, **299**, 2682–2684.
9 L. M. Jone, D. Dunham, M. Y. Rennie, J. Kirman, V. Lopez, K. C. Keim, W. Little, A. Gomez, J. Bourke, H. Ng, R. S. DaCosta and A. C. Smith, *Future Microbiol.*, 2020, **15**, 319–332.
10 V. Çakır, M. Goksel, M. Durmus and Z. Biyiklioglu, *Dyes Pigm.*, 2016, **125**, 414–425.
11 B. M. Amos-Tautua, S. P. Songca and O. S. Oluwafemi, *Molecules*, 2019, **24**, 2456.
12 Y. Nitzan, M. Gutterman, Z. Malik and B. Ehrenberg, *Photochem. Photobiol.*, 1992, **55**, 89–96.

13 S. M. Mahalingam, J. D. Ordaz and P. S. Low, *ACS Omega*, 2018, **3**, 6066–6074.
14 C. S. Oliveira, R. Turchiello, A. J. Kowaltowski, G. L. Indig and M. S. Baptista, *Free Radical Biol. Med.*, 2011, **51**, 824–833.
15 N. S. Gsponer, M. B. Spesia and E. N. Durantini, *Photodiagn. Photodyn. Ther.*, 2015, **12**, 67–75.
16 G. Jori, C. Fabris, M. Soncin, S. Ferro, O. Coppellotti, D. Dei, L. Fantett, G. Chiti and G. Roncucci, *Lasers Surg. Med.*, 2006, **38**, 468–481.
17 T. L. Collins, E. A. Markus, D. J. Hassett and J. B. Robinson, *Curr. Microbiol.*, 2010, **61**, 411–416.
18 H. Kurokawa, H. Ito, M. Inoue, K. Tabata, Y. Sato, K. Yamagata, S. Kizaka-Kondoh, T. Kadonosono, S. Yano, M. Inoue and T. Kamachi, *Sci. Rep.*, 2015, **5**, 10657.
19 N. Malatesti, I. Munitic and I. Jurak, *Biophys. Rev.*, 2017, **9**, 149–168.
20 Q. Deng, P. Sun, L. Zhang, Z. Liu, H. Wang, H. Ren and X. Qu, *Adv. Funct. Mater.*, 2019, **29**, 1903018–1903027.
21 L. Mamone, D. D. Ferreyra, L. Gándara, G. Di Venosa, P. Vallecorsa, D. Sáenz, G. Calvo, A. Batlle, F. Buzzola, E. N. Durantini and A. Casas, *J. Photochem. Photobiol., B*, 2016, **161**, 222–229.
22 S. K. Sharma, T. Dai, G. B. Kharkwal, Y. Huang, L. Huang, V. J. B. De Arce, G. P. Tegos and M. R. Hamblin, *Curr. Pharm. Des.*, 2011, **17**, 1303–1319.
23 C. A. Bristowa, R. Hudson, T. A. Paget and R. W. Boyle, *Photodiagn. Photodyn. Ther.*, 2006, **3**, 162–167.
24 L. C. Makola, S. Mgidlana and T. Nyokong, *Dyes Pigm.*, 2021, **192**, 109262.
25 S. Fery-Forgues and D. Lavabre, *J. Chem. Educ.*, 1999, **76**, 1260–1264.
26 J. S. Hsiao, B. P. Krueger, R. W. Wagner, T. E. Johnson, J. K. Delaney, D. C. Mauzerall, G. R. Fleming, J. S. Lindsey, D. F. Bocian and R. J. Donohoe, *J. Am. Chem. Soc.*, 1996, **118**, 11181–11193.
27 A. R. Da Silva, A. C. Pelegrino, A. C. Tedesco and R. A. Jorge, *J. Braz. Chem. Soc.*, 2008, **19**, 491–501.
28 N. A. Kuznetsova, N. S. Gretsova, V. M. Derkacheva, S. A. Mikhalenko, L. I. Solov'eva, O. A. Yuzhakova, O. L. Kaliya and E. A. Luk'yanets, *Russ. J. Gen. Chem.*, 2002, **72**, 300–306.
29 H. Y. Ammara and H. M. Badran, *Heliyon*, 2019, **5**, e02545.
30 M. Petersilka, U. J. Gossmann and E. K. U. Gross, *Phys. Rev. Lett.*, 1996, **76**, 1212–1215.
31 J. Frisch, G. W. Trucks, H. B. Schlegel, G. E. Scuseria, M. A. Robb, J. R. Cheeseman, G. Scalmani, V. Barone, B. Mennucci, G. A. Petersson, H. Nakatsuji, M. Caricato, X. Li, H. P. Hratchian, A. F. Izmaylov, J. Bloino, G. Zheng, J. L. Sonnenberg, M. Hada, M. Ehara, K. Toyota, R. Fukuda, J. Hasegawa, M. Ishida, T. T. Nakajima, Y. Honda, O. Kitao, H. Nakai, T. Vreven, J. A. Montgomery, Jr, J. E. Peralta, F. Ogliaro, M. Bearpark, J. J. Heyd, E. Brothers, K. N. Kudin, V. N. Staroverov, R. Kobayashi, J. Normand, K. Raghavachari, A. Rendell, J. C. Burant, S. S. Iyengar, J. Tomasi, M. Cossi, N. Rega, J. M. Millam, M. Klene, J. E. Knox, J. B. Cross, V. Bakken, C. Adamo, J. Jaramillo, R. Gomperts, R. E. Stratmann, O. Yazyev, A. J. Austin, R. Cammi, C. Pomelli, J. W. Ochterski, R. L. Martin, K. Morokuma, V. G. Zakrzewski, G. A. Voth, P. Salvador, J. J. Dannenberg, S. Dapprich, A. D. Daniels, Ö. Farkas, J. B. Foresman, J. V. Ortiz and J. Cioslowski, D. J. Fox, *Gaussian 09*, Gaussian, Inc., Wallingford CT, 2009.
32 Y. I. Openda, B. P. Ngoy and T. Nyokong, *Front. Chem.*, 2021, **9**, 628316.
33 O. L. Osifeko, M. Durmus and T. Nyokong, *J. Photochem. Photobiol., A*, 2015, **301**, 47–54.
34 Y. I. Openda and T. Nyokong, *J. Photochem. Photobiol., A*, 2021, **411**, 113200.
35 W.-C. Lin, K. Brondum, C. W. Monroe and M. A. Burns, *Sensors*, 2017, **17**, 1655.
36 Z. Liang, H.-Y. Wang, H. Zheng, W. I. Zhang and R. Cao, *Chem. Soc. Rev.*, 2021, **50**, 2540.
37 M. Uttamlal and A. S. Holmes-Smith, *Chem. Phys. Lett.*, 2008, **454**, 223–228.
38 E. Gürel, M. Piskin, S. Altun, Z. Odabas and M. Durmus, *Dalton Trans.*, 2015, **44**, 6202–6211.
39 D. Topkaya, S. Y. Ng, Y. Bretonniere, D. Lafont, L. Y. Chung, H. B. Lee and F. Dumoulin, *Photodiagn. Photodyn. Ther.*, 2017, **17**, A61.
40 T. Nyokong, *Coord. Chem. Rev.*, 2007, **251**, 1707–1722.
41 K. N. Solov'ev and E. A. Borisevich, *Phys.-Usp.*, 2005, **48**, 231–253.
42 H. Ramesh, T. Mayr, M. Hobisch, S. Borisov, I. Klimant, U. Krühne and J. M. Woodley, *J. Chem. Technol. Biotechnol.*, 2016, **91**, 832–836.
43 N. M. Barbosa Neto, D. S. Correa, L. De Boni, G. G. Parra, L. Misoguti, C. R. Mendonca, E. I. Borissevitch, S. C. Zilio and P. J. Goncalves, *Chem. Phys. Lett.*, 2013, **587**, 118–123.
44 M. Enescu, K. Steenkeste, F. Tfibel and M. P. Fontaine-Aupart, *Chem. Phys.*, 2002, **4**, 6092–6099.
45 Z. Biyiklioglu, I. Ozturk, T. Arslan, A. Tunçel, K. Ocakoglu, M. Hosgor-Limoncu and F. Yurt, *Dyes Pigm.*, 2019, **166**, 149–158.
46 B. W. Handerson, D. A. Bellnier, W. R. Greco, A. Sharma, R. K. Pandey, L. A. Vaughan, K. R. Weishaupt and T. J. Daugherty, *Cancer Res.*, 1997, **15**, 4000–4007.
47 N. Malatesti, A. Harej, S. P. Kraljevic, M. Loncaric, H. Zorc, K. Wittine, U. Andelkovic and D. Josic, *Photodiagn. Photodyn. Ther.*, 2016, **15**, 115–126.
48 D. A. Caminos, M. B. Spesia, P. Pons and E. N. Durantini, *Photochem. Photobiol. Sci.*, 2008, **7**, 1071–1078.
49 F. M. Engelmann, I. Mayer, D. S. Gabrielli, H. E. Toma, A. J. Kowaltowsk, K. Araki and M. S. Baptista, *J. Bioenerg. Biomembr.*, 2007, **39**, 175–185.
50 T. S. Beveridge, *J. Bacteriol.*, 1999, **181**, 4725–4733.
51 P. D. Martino, *AIMS Microbiol.*, 2018, **4**, 274–288.
52 Y. I. Openda, R. Matshitse and T. Nyokong, *Photochem. Photobiol. Sci.*, 2020, **19**, 1442–1454.
53 A. P. Ribeiro, M. C. Andrade, J. D. Silva, F. L. Primo, A. C. Tedesco, A. C. Tedesco and A. C. Pavarina, *Photochem. Photobiol.*, 2013, **89**, 111–119.
54 I. B. Rosseti, L. R. Chagas and M. S. Costa, *Lasers Med. Sci.*, 2014, **29**, 1059–1064.